Quaternary International 718 (2025) 109647

Contents lists available at ScienceDirect

Quaternary International

journal homepage: www.elsevier.com/locate/quaint

Solar forcing as driver for late Holocene rainfall intensity in the Peruvian Andes

Karsten Schittek [a,*], Jan Wowrek [a], Nicolas Käuffer [a], Markus Reindel [b], Bertil Mächtle [c]

[a] Institute of Geography Education, University of Cologne, Cologne, Germany
[b] German Archaeological Institute, Bonn, Germany
[c] Geographical Institute, Heidelberg University, Heidelberg, Germany

ARTICLE INFO

Keywords:
Solar forcing
Little ice age
South American summer monsoon
Late holocene
Paleoclimate
Pollen
Tropical andes

ABSTRACT

This study presents a high-resolution palaeoclimate record from sediment cores collected from the siltation area of Laguna Comercocha (LC) in southern Peru, spanning the last 1070 cal years. The primary objective was to investigate climatic variations and environmental changes before, during and after the Little Ice Age (LIA) in the central Andes, with particular emphasis on precipitation patterns and their relation to solar forcing. The extracted core provided a continuous sedimentary archive, offering insights into climate variability on sub-centennial to inter-decadal timescales. The methodology included analysing the sediment cores using X-ray fluorescence (XRF) to measure the concentrations of allogenic elements such as titanium (Ti), silicon (Si), potassium (K), iron (Fe) and calcium (Ca). Ti/coh ratios served as proxy for effective rainfall and runoff from the local catchment. In addition, pollen and non-pollen palynomorphs (NPPs) were identified and quantified to reconstruct past vegetation and climatic conditions. The study revealed that lithogenic input to the LC increased significantly after 1150 cal yr AD, likely due to increased precipitation. In particular, periods of increased lithogenic input were identified during the LIA, corresponding to solar minima and pointing to solar forcing as a major driver of precipitation changes in the central Andes.

1. Introduction

The Little Ice Age (LIA) was a period of increased global temperature and precipitation variability that lasted from approximately 1250-1850 A.D. (Solomina et al., 2015; Autin et al., 2022; Wanner et al., 2011). Proxy climate records from many locations (Jones and Mann, 2004) and climate simulations of varying complexity (see Jomelli et al., 2022) suggest that the LIA was a global event, marked by the advance of glaciers worldwide. However, the magnitude and the precise timing of the glacial advances varied significantly by region (Mann et al., 2009).

Understanding the factors responsible for this Holocene cold event and the associated environmental impacts is crucial for comprehending the complexity of the climate system and its sensitivity to external forcing. Over tropical South America, proxy climate records such as ice cores, tree rings, sediments, speleothems and glacier sensitivity analyses (e.g. Thompson et al., 2006; Polissar et al., 2006; Reutter et al., 2009; Morales et al., 2012; Jomelli et al., 2022) provide a range of paleoclimate data over the LIA timescale. For instance, Autin et al. (2022) found that, based on an investigation of the Zongo glacier in Bolivia, annual precipitation was about 20% higher than today, with temperatures 1.1 °C cooler. Polissar et al. (2006) emphasized the strong influence of solar activity on century-scale tropical climate variability during the late Holocene.

Solar irradiation is the primary driver for all climatic circulation processes on Earth (Steinhilber et al., 2009). Evidence for a direct solar influence on the Earth's climate has been growing due to the increasing continuity, length and resolution of paleoclimate reconstructions (Varma et al., 2011; Carozza et al., 2014; Brehm et al., 2021). Reconstructions of total solar irradiance show that the LIA included intervals of lower solar irradiance ("solar minima") that were repeatedly interrupted by warmer phases (Brehm et al., 2021; Wanner et al., 2022). However, proxy data from tropical South America related to external forcing factors remain sparse. To better understand climate variability of this region, continuous high-resolution archives are necessary to resolve the temporal and spatial patterns during the late Holocene.

We present a sediment record from the peaty siltation area of Laguna Comercocha (LC) in southern Peru, providing new high-resolution evidence of climate variability from just before the onset of the LIA. Our

* Corresponding author.
E-mail address: schittek@uni-koeln.de (K. Schittek).

https://doi.org/10.1016/j.quaint.2024.109647
Received 4 August 2024; Received in revised form 13 November 2024; Accepted 18 December 2024
Available online 9 January 2025

primary goal is to reconstruct late Holocene precipitation changes to enhance understanding of sub-centennial to inter-decadal climate variability in the central tropical Andes, where high-resolution terrestrial climate proxy records are scarce. Here, we present a well-dated peat/organic sediment record covering the last 1070 cal years BP, utilizing high-resolution geochemical and pollen data to support our interpretations. The continuous nature of the peat/organic sediment record allows us to detect changes in lithic influx and to determine the timing of these events.

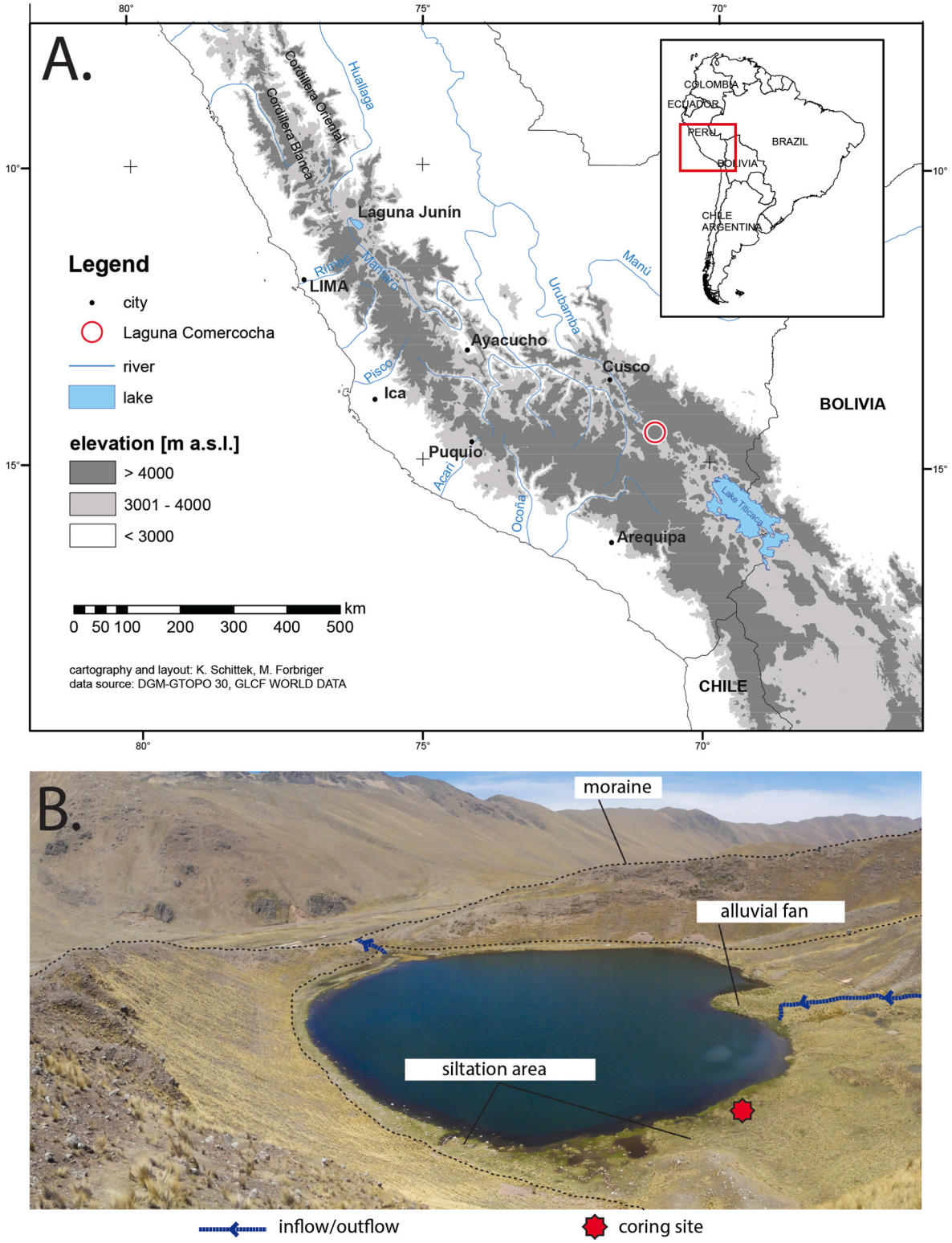

Fig. 1. A. Location of the LC study area (red circle). B. Laguna Comercocha with Pleistocene moraine and location of the coring site. (For interpretation of the references to colour in this figure legend, the reader is referred to the Web version of this article.)

2. Geographical location, regional climate and vegetation

The studied wetland is located in the siltation area of Laguna Comercocha (14°28′S, 70°59′W; Fig. 1) in the Vilcanota valley, southern Peru. This glacial lake is located at an elevation of 4345 m a.s.l. within the mountain pass "Abra de la Raya" on the border between the departments of Cusco and Puno. During the Pleistocene, a southwest-facing glacier formed a tongue-shaped basin with steep moraines near the summit of Nevado Cunca (~5.300 m a.s.l.). After deglaciation, Laguna Comercocha formed in the basin, surrounded by a moraine wall to the east, west and south, interrupted by an outlet to the south. The moraine walls and sediments are composed of granitic rocks of the footwall, belonging to the La Raya formation of the Palaeogene, and clastic and volcanoclastic rocks of the hanging wall, belonging to the Mitu group of the upper Permian (Sanchez and Zapata, 2003). Between the moraine wall and the lake, in the southern, eastern and western direction, there is a lake siltation area, which is dominated by peat-accumulating vegetation.

The climate at Laguna Comercocha has the characteristics of a diurnal tropical mountain climate (Fig. 2). Average temperatures show minimal variation throughout the year. During the Southern Hemisphere summer, temperatures rise to over 6 °C in January due to increased radiation, but average temperatures never fall below freezing. The average annual temperature is 4.2 °C.

The intra-annual climate variability in the Andes is driven by the South American Summer Monsoon (SASM), which is characterized by seasonal meridional shifts. The Intertropical Convergence Zone (ITCZ), which reaches its northernmost position during the winter months of June, July, and August (JJA), triggers a dry season in central South America due to reduced convective precipitation. As the year progresses, the ITCZ shifts towards the central Amazon basin, initiating the SASM (Garreaud and Aceituno, 2007). The South Atlantic Convergence Zone, which extends from the central Amazon basin to the southeast coast of Brazil, is characterized by strong convective precipitation and high cloud cover (Vera et al., 2006). In the arid region of the Altiplano Plateau, precipitation variability is primarily influenced not by local convective variability, but by changes in the dominant wind direction, which affects large-scale moisture transport conditions (Garreaud et al., 2003).

During JJA, when the ITCZ is at its northernmost position, westerly winds prevail in the upper troposphere at 200 hPa (Garreaud and Aceituno, 2007). As a result, dry winds are enhanced in the lower troposphere, leading to dry conditions in the Southern Hemisphere winter (Garreaud et al., 2003). In contrast, during the summer months of December, January, and February, enhanced cumulus convection over the Amazon basin releases heat to form an upper-level high known as the Bolivian High (BH). Located at 15°S and 65°W, the BH induces a change in wind direction, resulting in easterly winds towards the Andean region (Garreaud and Aceituno, 2007). The formation of the BH is also associated with the presence of the Low-Level Jet (LLJ), a southwestward directed wind band along the eastern slopes of the Andes in the lower troposphere (Segura et al., 2020). These winds transport convective rain clouds in mesoscale, spatially coherent patterns across the Andes (Garreaud et al., 2003). These clouds, enriched with moisture from the Amazon, cause intra-seasonal precipitation events, resulting in rain episodes lasting one to two weeks, followed by dry periods of similar duration. Due to these periodic summer rains, 60 % of the Altiplano's precipitation falls between December to January (Garreaud and Aceituno, 2001).

In principle, the decrease in temperature with increasing altitude finds its expression in the formation of vertical vegetation zones (Körner, 2012). However, pollen archives in the dry central Andes indicate that vegetation is much more sensitive to precipitation, as moisture availability is the limiting factor for plant growth (Flantua et al., 2016). This finds its direct expression in the vegetation surrounding the LC.

The highest vegetation zone described by Graf (1981) is the subnival belt (4500–5300 m a. s. l.). At higher elevations, plant growth is largely inhibited by permafrost and snow cover. Plants at these elevations are adapted to daily night frosts, low average annual temperatures and short growing seasons. The plant communities are sparsely vegetated (<50% coverage), dominated by tussock grasses (mostly *Festuca* and *Deyeuxia*) and dwarf shrubs (e.g. *Baccharis, Senecio, Xenophyllum*). Between approx. 3700/3800 and 4500 m a. s. l., the upland areas are dominated by a dense steppe of tussock grasses, interspersed by Asteraceae occurring as shrubs. Other (dwarf) shrubs include *Ephedra*, Fabaceae (*Adesmia, Astragalus*), Rosaceae (*Tetraglochin*) and Solanaceae (*Fabiana*).

During fieldwork, vegetation surveys identified the following taxa on the lake's sedimentation area: *Cardamine bonariensis, Cotula mexicana,*

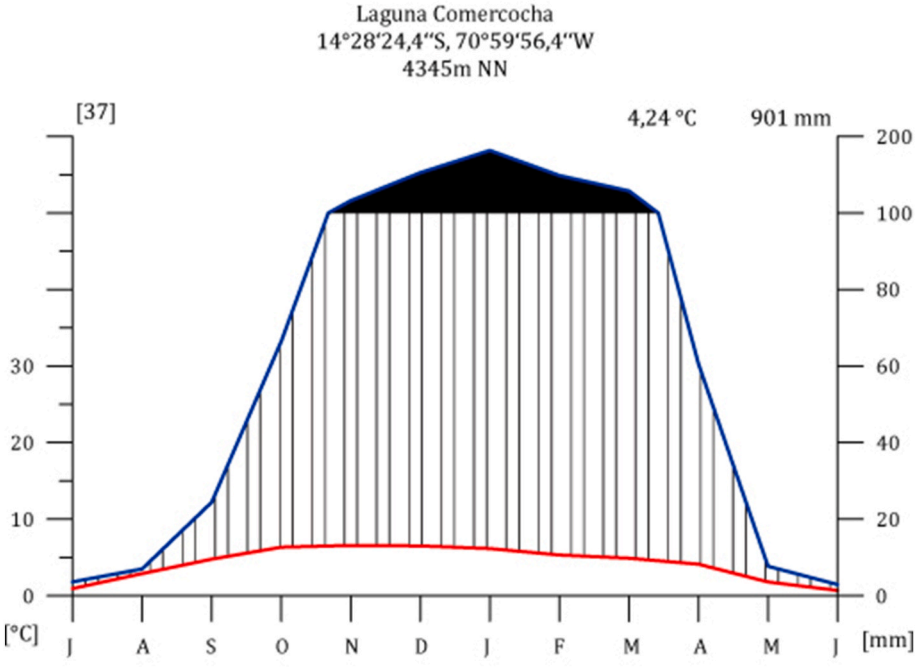

Fig. 2. Climate diagram Laguna Comercocha (data source: Climate Reanalyzer. Based on CFSR data (1979–2015). http://cci-reanalyzer.org).

Eleocharis tucumanensis, Lachemilla diplophylla, Lilaeopsis macloviana. The surrounding cushion-plant peatland revealed species including: *Aciachne pulvinata, Baccharis serpyllifolia, Calandrinia spec., Callitriche spec., Carex spec., Deyeuxia curvula, Deyeuxia eminens, Deyeuxia rigescens, Distichia muscoides, Festuca humilior, Gentiana prostrata, Hypochoeris taraxacoides, Juncus spec., Lachemilla pinnata, Lemna spec., Lobelia oligophylla, Oritrophium limnophyllum, Ourisia muscosa, Plantago tubulosa, Ranunculus psychrophilus, Senecio breviscapus, Viola spec., Werneria pygmaea, Zameioscirpus muticus.* These plant species are typical components of the azonal high-Andean wetland and peatland vegetation (Ruthsatz, 2012).

3. Methods

A peat-accumulating siltation area on the eastern shore in the central area of the glacial cirque was selected for drilling. The drilling site is located close to the lake shore. However, since the lake has recently been dammed at its natural outlet, it can be assumed that the lake level was slightly lower before the dam was built. Fieldwork at LC was carried out in October 2011. Sediment cores were collected to a total depth of 180 cm using a short core drill suitable for the fibrous Andean (cushion-plant) peat (Schittek, 2014). In this paper we report on the upper 60 cm of the 180 cm sediment sequence recovered in core P118C.

At the Paleoecology Laboratory of the Institute of Geography Education (University of Cologne), the core was split into two core halves, photographed and sedimentologically described. To obtain qualitative elemental counts for major and trace elements, one half of the core was analysed with an ITRAX X-ray fluorescence (XRF) core scanner (Cox Analytical Systems; Croudace et al., 2006) at GEOPOLAR (University of Bremen) at a resolution of 2 mm. XRF scanning was performed using a molybdenum (Mo) tube at 20 kV and 10 mA, with an exposure time of 10 s per measurement. The results are expressed as counts (cnts) and only elements over 100 cnts were selected. Titanium (Ti), silicium (Si), potassium (K), iron (Fe) and calcium (Ca) were chosen for interpretation.

Ti is an element that is not anchored in any autogenic biological processes and can therefore be considered as an element of purely allogenic origin (Muller et al., 2008; Rothwell and Croudace, 2015). As igneous Ti-bearing minerals are known to be progressively dissolved during silicate rocks weathering, leached Ti is efficiently released with runoff (White et al., 1994; Novoselov et al., 2020). To account for possible dilution effects of the XRF signal by organic matter, we used normalization of the measured Ti values against the coherent (coh) scatterplots (Ohlendorf et al., 2013). Fe was normalized to Ti to better reflect variations in autogenous redox dynamics within the groundwater-influenced siltation area (Schittek et al., 2016; Thomson et al., 2006). Ca is considered to reflect increased evaporation and secondary precipitation of gypsum within the organic sediment (Kock et al., 2019).

The other half of the core was sub-sampled at 2 cm intervals (or less, depending on the stratigraphy) for pollen analysis. For pollen sample preparation, the volume of all samples was determined and a known number of *Lycopodium* markers were added. Further pollen preparation followed the standard techniques described in Faegri and Iversen (1989). Pollen samples were mounted in glycerine and pollen types were counted under ×400 and ×1000 magnification. A minimum of 300 regional pollen types were counted in each sample. The identification of pollen and non-pollen palynomorphs (NPPs) was carried out using the institute's own reference collection, the reference collection of the Laboratorio de Palinología (Universidad Nacional de Jujuy) as well as the atlases and identification keys of Heusser (1971), Markgraf and D'Antoni (1978), Graf (1979), Wingenroth and Heusser (1985), Taugourdeau (2006), Sandoval et al. (2010) and Torres et al. (2012). The percentages of pollen types refer to the total sum of all pollen types counted, excluding the aquatic/semi-aquatic pollen types. The percentages of (semi-)aquatic pollen types are based on the total sum of all (semi-)aquatic and all terrestrial types. All NPP are given in their concentration (n/cm^3). Pollen cluster analysis was performed with CONISS ("Constrained cluster analysis by sum-of-squares") (Grimm, 1987), including all terrestrial pollen types, with abundances of >5% of total pollen.

Detailed age control is based on a series of 6 AMS ^{14}C dates of plant remains, measured at Curt Engelhorn Centre for Archaeometry, Mannheim (5), and Poznan Radiocarbon Laboratory (1) (Table 1). The INTCAL20 data set for Northern Hemisphere calibration (Reimer et al., 2020) was applied because during the austral spring and summer seasons, the south shift in the ITCZ brings atmospheric CO_2 from the Northern Hemisphere to the Andes, which is taken up by the vegetation during the growing season. The peat surface (2011 AD) was used as an additional tie point. The age model was calculated with the Bacon age-modelling software 'rbacon', version 2.5.3 (Blaauw and Christen, 2011) in the statistical software package "R" (R Core Development Team, 2013). To test the correlation between unevenly spaced time series of different paleoclimate records, the BINCOR 0.2 package was used (Polanco-Martínez et al., 2019).

4. Results

4.1. Chronology, lithology and XRF analysis

The 60 cm-long sequence presented in this paper spans the last 1070 cal years and shows a constant sediment accumulation rate with an average resolution of 20 years per centimeter (Fig. 3). The highest resolution of ~14 yr cm^{-1} occurs at 40–60 cm depth, while the lowest resolution is in the upper 20 cm of the core (~26–27 yr cm^{-1}). The complete 180 cm-long core, which was extracted at LC, reaches back to 7533 cal yr BP (not shown in this paper).

Deposits in the LC silting zone consist of peat layers and layers of clayey/silty organic sediment in varying proportions. The top 4.5 cm of the sequence consists of peat with undecomposed plant remains. At 4.5–5.5 cm there is a layer of clayey silt. From 5.5 to 24 cm the sequence consists of clayey sediments. These are initially greyish (7–9 cm), then lighter and increasingly interspersed with rust concretions and plant remains (9–19 cm), and finally brownish with plant remains and isolated rust concretions (19–24 cm).

From 24 cm the sediment consists of dark brown silty clay interspersed with plant remains. The section of 36–50.5 cm consists of a partly laminated alternation between more mineral (clayey silt) and organic (peat) layers. The final section (50.5–60 cm) of the core profile consists of dark, undecomposed peat.

The XRF count rates detect changes in lithogenic influx and therefore allow to fingerprint the stratigraphic characteristics of the sediment matrix (Van der Bilt et al., 2015). Key elements such as Ti, Si, K and Fe show noteable variations (Fig. 4). These lithogenic elements, originating from the bedrock in the small watershed, indicate increased lithic flux during periods of heightened precipitation. The hydrological changes coupled with climate dynamics can modulate the extent of terrigenous input into the siltation area. Thus, the Ti/coh ratio serves as an indirect indicator of precipitation (Martel-Cea et al., 2023; Schittek et al., 2016).

The lower part of the LC core is characterized by moderate variations and intermediate element counts. In contrast, the upper 30 cm display

Table 1
Radiocarbon ages of core P118C. All dates were measured on plant remains.

Sample depth	Lab. no.	Age^{14}C/error
21,5-22	MAMS-47852	374 ± 21 BP
25-25,5	Poz-79527	705 ± 30 BP
42-42,5	MAMS-14769	996 ± 26 BP
56-56,5	MAMS-47854	1091 ± 19 BP
102-102,5	MAMS-47855	1804 ± 31 BP
113-113,5	MAMS-47856	1923 ± 22 BP

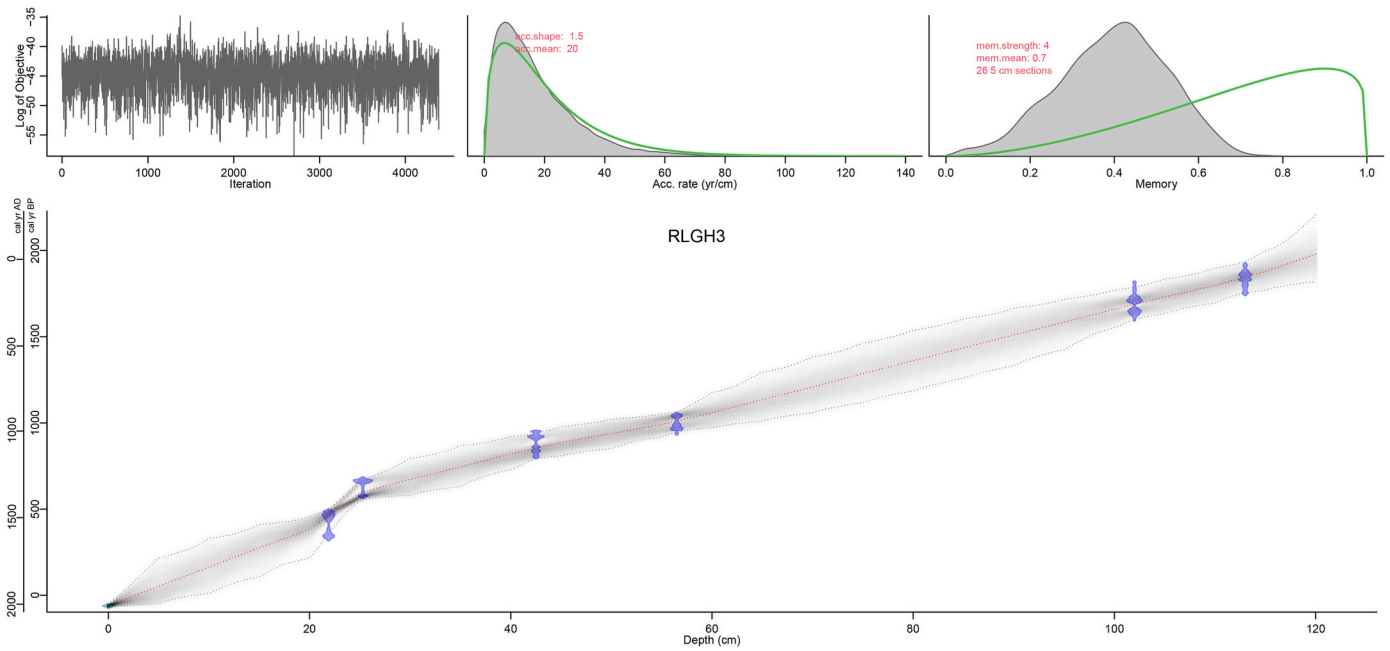

Fig. 3. Bacon age-depth model for the LC composite profile. Upper panels depict the Markov Chain Monte Carlo (MCMC) iterations (left), the prior (green curves) and posterior (grey histograms) distributions for the accumulation rate (middle panel) and memory (right panel). The bottom panel shows the calibrated 14C dates (light blue) and the age-depth model (red curve) with 95% confidence intervals (grey dotted lines). (For interpretation of the references to colour in this figure legend, the reader is referred to the Web version of this article.)

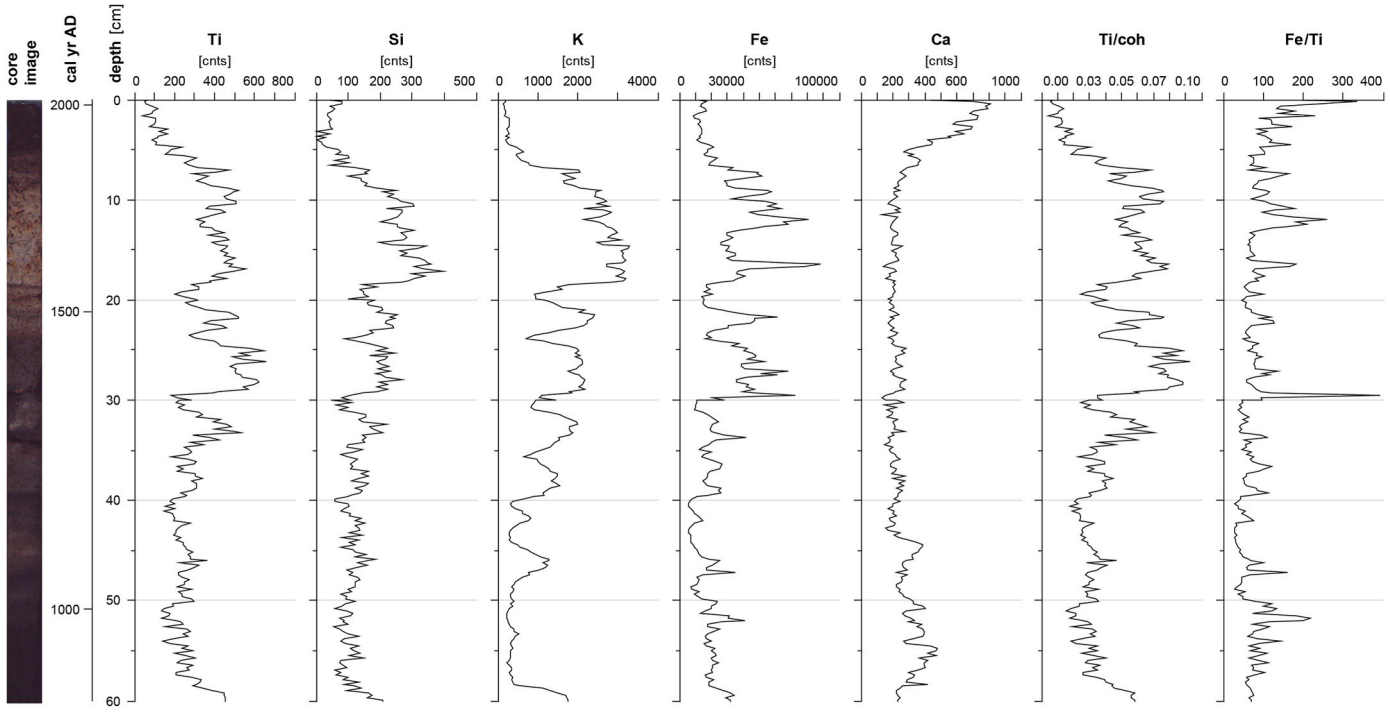

Fig. 4. Results of XRF analysis with core image. Given are Ti, Si, K, Fe and Ca values as well as the Ti/coh ratio and the Fe/Ti ratio.

absolute maxima of element counts and marked fluctuations with distinct switches between high and low values. Throughout the 1070-year sediment record, Ti/coh values were generally low between 900 and 1250 cal yr AD, during the Medieval Climate Anomaly (MCA). The amplitude of fluctuations increases significantly with the onset of the LIA around 1250 cal yr AD, peaking at 1280–1400, 1450–1520 and 1620–1880 cal yr AD. Pronounced minima in Ti/coh ratios during the LIA occur around 1270, 1420–1460 and 1540–1600 cal yr AD. From 1900 cal yr AD to the present, Ti/coh values reach the lowest level in the entire record, corresponding with sediments characterized by high organic content and reduced allogenic input.

Changes in Ca counts and Fe/Ti ratios indicate *in situ* redox condition changes due to water table fluctuations. Both parameters show highest values at the lower section and top sections of the record, Fe/Ti ratios characterized by high fluctuation throughout.

4.2. Pollen analysis

The pollen record (Fig. 5) reflects the typical regional vegetation of the Altoandean and Puna elevational belts (Graf, 1981, 1986). A total of 29 different pollen types were identified and documented in 30 samples. Poaceae dominate the pollen spectrum, comprising 52–95 % of the regional pollen assemblage, with only four samples below 70 % abundance. Among other pollen types, only *Senecio*-type Asteraceae frequently exceed 10 % abundance (max. 29 %). Cyperaceae, *Plantago*, Gentianaceae and *Sisyrinchium*, representing local peatland and semi-aquatic vegetation (Ruthsatz, 2012), were excluded from the pollen sum. Other pollen types include tree pollen from *Alnus* and *Polylepis* from the eastern Andean forests below 3500 m a.s.l., which occur in low abundances. Additionally, *Isoetes* and fern spores (excluding *Lycopodium*) were counted. Coprophilous fungal spores (*Byssothecium*, *Sordaria* and *Brachysporium*), indicating intensive grazing, and *Glomus* fungal spores, indicating soil erosion, represent further microfossils other than pollen.

Based on the analysis of the pollen types with a minimum abundance of 5 %, cluster analysis allows the differentiation of the data into 6 pollen zones. Zone 1.1 (46.5–60 cm) is dominated by Poaceae. Their abundance never falls below 88 %, while *Senecio*-type Asteraceae do not exceed 2.2 %. Cyperaceae increase significantly in the sample adjacent to the next pollen zone. Ferns occur only in the upper part of the zone. *Byssothecium* and *Glomus* are also highly abundant.

In zone 1.2 (39–46.5 cm) the Poaceae lose their dominance and the proportion of *Senecio*-type Asteraceae increases significantly with an average of 8.5 %. In the middle of this section, at a depth of 42.6 cm, *Senecio*-type Asteraceae (11.6 %), Apiaceae (3.9 %) and *Astragalus*-type Fabaceae (1.6 %) reach their maxima, while Poaceae drop to the lowest value (78.9 %) within the zone. Cyperaceae and *Plantago*, representing the local semi-aquatic vegetation, also increase in abundance. *Byssothecium* and *Glomus* show lower concentrations than before.

In pollen zone 1.3 (26.1–39 cm) the *Senecio*-type Asteraceae, Cyperaceae and *Plantago* remain abundant, but lose their dominance in favor of the Poaceae, which are represented with at least 92 % at 30.6–38.8 cm. While Apiaceae are sporadically documented, the *Astragalus*-type Fabaceae is no longer present. In the upper samples of the zone (27.2–29.4 cm), *Senecio*-type Asteraceae, Apiaceae, Cyperaceae and *Plantago* regain abundance, while the proportion of Poaceae drops to below 85%. The concentration of ferns increases throughout the zone. *Byssothecium* is missing in the top and bottom samples of the zone, but is otherwise present throughout the zone.

Zone 2.1 (19.4–26.1 cm) comprises three counted samples (and is similar to zone 1.2). The dominance of Poaceae decreases significantly and is still represented by an average of 65.9 %, while the abundance of *Senecio*-type Asteraceae, Apiaceae, *Astragalus*-type Fabaceae, Cyperaceae and *Plantago* increases. *Senecio*-type Asteraceae (17.8 %) and *Astragalus*-type Fabaceae (10.7 %) reach their maxima at 20.6 cm. The NPP tend to occur in low concentrations. The ferns decrease to lower concentrations. Only *Glomus* occurs in higher concentrations.

Zone 2.2 (13–19.4 cm) is characterized by very high percentages of Poaceae, accompanied by low percentages of *Senecio*-type Asteraceae. The local semi-aquatic vegetation is rather less represented. At 18.3 cm *Alnus* reaches its maximum of 1.4 % and Brassicaceae 4.5 %. NPP are hardly present in this zone.

In the youngest zone 2.3 (0–13 cm), Apiaceae and *Astragalus*-type Fabaceae increase in abundance together with *Senecio*-type Asteraceae, while the abundance of Poaceae decreases to 52 %, increases to 95 %, and decreases again to 78 % in the top layer. The local semi-aquatic vegetation continuously increases to higher abundances. The NPP, especially *Sordaria*, *Brachysporium* and *Glomus*, all show higher concentrations in the uppermost samples.

5. Discussion

5.1. Past environmental changes at Laguna Comercocha

The siltation area of Laguna Comercocha represents a precise sediment trap that provides an opportunity to obtain a continuous paleoclimate archive for the study of climate changes on sub-centennial to inter-decadal time scales. The LC record provides new high-resolution evidence of climate variability before, during and after the LIA in South America. This study shows that the magnitude of lithic influx from the small and steep, sparsely vegetated watershed of the LC is linked to changes in precipitation intensity. Increased allogenic sediment

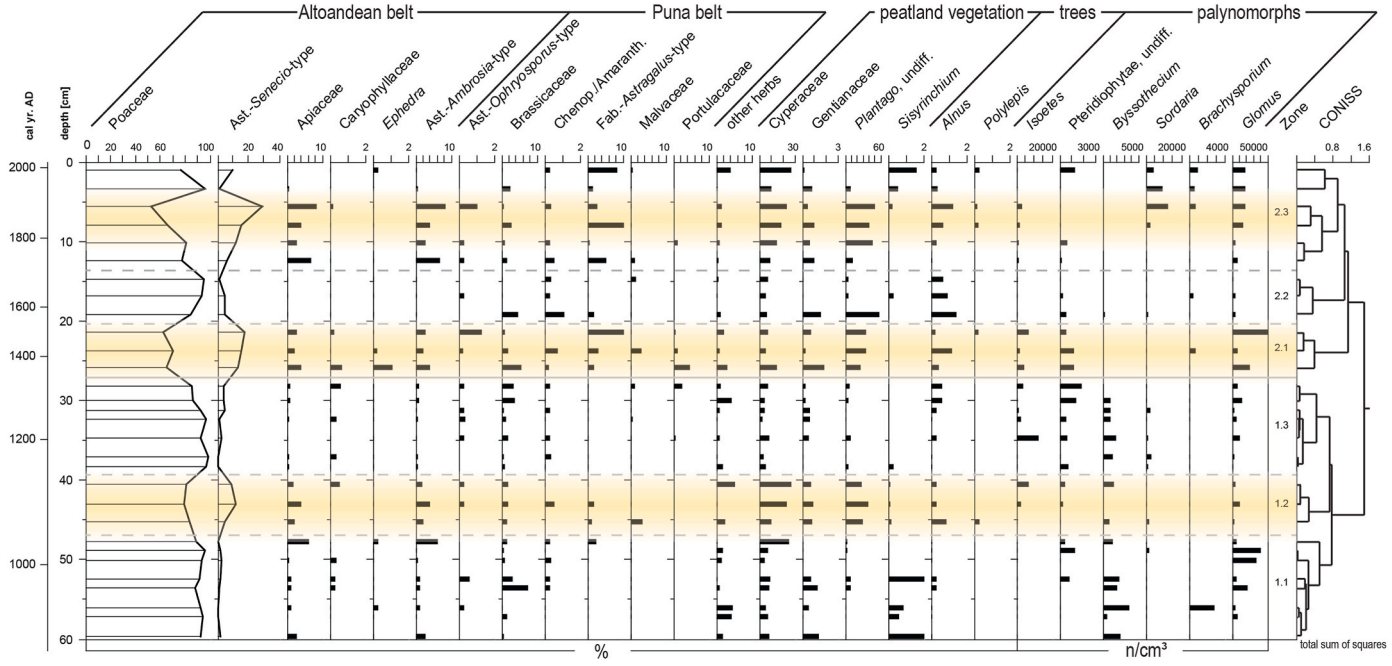

Fig. 5. Pollen and palynomorphs diagram. Peatland (semi-aquatic) vegetation was excluded from the pollen sum. Yellow bars represent dry periods. (For interpretation of the references to colour in this figure legend, the reader is referred to the Web version of this article.)

accumulation in the peat matrix occurred during the solar minima of the LIA. Hence, our study reveals evidence that precipitation changes in the south-eastern Peruvian Andes are linked to variations in solar activity during the LIA (Fig. 6).

Ti as a proxy for effective precipitation and runoff from local watersheds has been successfully applied in a number of studies (Martel-Cea et al., 2023; Van der Bilt et al., 2015, 2017; Balascio et al., 2011; Metcalfe et al., 2010). At LC, the Ti/coh ratio clearly identifies periods when the siltation area was influenced by the input of allogenic lithic material originating from the catchment area. Thus, stratigraphic analysis of the peat/organic sediment column allows inferences to be made about the intensity of weathering and erosional processes, and hence can be linked to past environmental changes (Schittek et al., 2021).

Lithogenic input to the LC begins to increase after 1150 cal yr AD, indicating a change in geomorphodynamics. We propose that the first

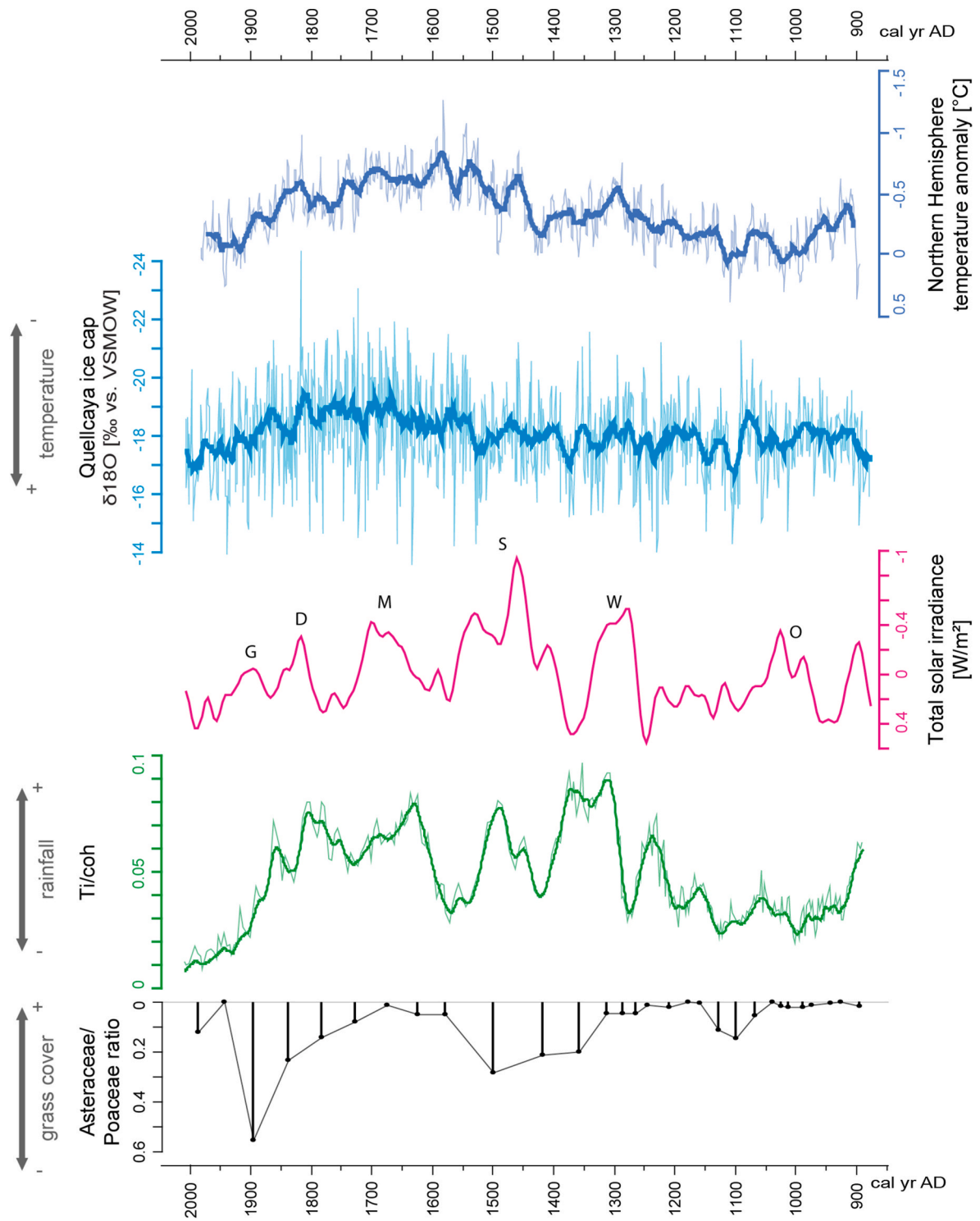

Fig. 6. The late Holocene Ti/coh ratio and *Senecio*-type Asteraceae/Poaceae pollen ratio sequences of the LC compared with total solar irradiance (Steinhilber et al., 2009), $\delta^{18}O$ (‰ vs. VSMOW) of Quellcaya ice cap, Peru (Thompson et al., 2013) and Northern Hemisphere temperature reconstruction (Moberg et al., 2005). Fat lines show 21-year averages. Capital letters mark the solar minima of the LIA (G: Gleissberg, D: Dalton, M: Maunder, S: Spörer, W: Wolf, O: Oort).

prolonged episode of lithogenic input between 1280 and 1400 cal yr AD marks the onset of a period of sustained heavier rainfall. The timing of this climatic change coincides with an intensification of the SASM (Vuille et al., 2012; Bird et al., 2011; Rodbell et al., 2008) and evidence of glacial advance in the Peruvian Andes (Stroup et al., 2014; Stansell et al., 2013; Thompson et al., 1986, 2013; Licciardi et al., 2009). Ice accumulation at the Quelccaya ice cap increased after 1350 cal yr AD, indicating a significant decrease in temperature (Thompson et al., 1986, 2013). The Ti/coh ratio in the LC record peaks at 1450–1520, 1600–1750, 1780–1820 and 1840–1850 cal yr AD. These peaks show striking agreement with LIA-related research in South America (e.g. Licciardi et al., 2009; Varma et al., 2011; Polissar et al., 2006) and interhemispheric approaches to temperature variability during the late Holocene (e.g. Jomelli et al., 2022; Moffa-Sánchez et al., 2014; Mann et al., 2009). The LC record therefore clearly confirms interhemispheric climate linkages.

Pollen analysis basically confirms the XRF results. The abundant presence of Poaceae pollen reflects very well the predominance of grasses in the Altoandean elevational vegetation belt. The sweet grasses are typical shallow-rooted plants whose spread is favored by humid conditions (Liu et al., 2005). Grass cover density decreases during less humid periods and better adapted upland vegetation components such as Asteraceae (mostly *Senecio*-type), Apiaceae, Brassicaceae and Malvaceae become more prominent in the pollen spectrum. In various palaeoenvironmental studies of the central Andes at similar latitudes, high Poaceae abundances are interpreted as indicators of humid climatic conditions (Schittek et al., 2015, 2018; Ledru et al., 2013; Kuentz et al., 2012; Liu et al., 2005; Graf, 1981, 1986). Based on pollen evidence, drier periods are highlighted for 1100–1150, 1350–1550 and around 1900 cal yr AD in the LC sequence.

However, during the late Holocene, the vegetation cover in high-Andean environments (dominated by grasses) was subject to widespread and locally intensive grazing by llamas and alpakas (and later sheep, cows, donkeys and horses). The indicator value of grass pollen may therefore become less reliable as population pressure increases. A clear indication of the presence of grazing animals is provided by the high concentrations of spores of the coprophilous fungi *Sordaria* and *Brachysporium* in the youngest layers of the core profile.

5.2. Solar forcing and climate linkages

Changes in humidity associated with changes of the strength of the SASM have been demonstrated by several studies in the Peruvian Andes (e.g. Arnold et al., 2021; Campos et al., 2022; Jara et al., 2020; Novello et al., 2018; Schittek et al., 2018, 2016; Bustamante et al., 2016; Stroup et al., 2014; Vuille et al., 2012; Bird et al., 2011; Reutter et al., 2009), all confirming the transition from a warmer and drier climate during the MCA towards a significantly cooler and wetter climate during the LIA.

Vuille et al. (2012) demonstrate a link between the conditions in the Northern Hemisphere (NH) and the Southern Hemisphere (SH) on a multidecadal scale by analysing different paleoclimatic studies in South America. The researchers emphasize the importance of the relationship between colder or warmer temperatures in the NH and warmer or colder temperatures in the SH. They show that changes in North Atlantic sea surface temperature and the resulting cooling of the NH lead to a more southerly position of the ITCZ. This southward shift intensifies SASM, independent of local and regional forcing. Variability in North Atlantic sea surface temperatures is linked to the North Atlantic Oscillation (NAO) (Arnold et al., 2021). This leads to changes in wind speed, temperature, and moisture transport (Hurrell et al., 2001). During its positive phase, the NAO intensifies the Atlantic Meridional Overturning Circulation (AMOC) (Arnold et al., 2021), a key component of the thermohaline circulation that has a central influence on the ITCZ through meridional heat distribution (Kuhlbrodt et al., 2007). An increased meridional sea level pressure and sea surface temperature gradient, together with an enhanced AMOC, generate north winds that cross the equator. As a result, the ITCZ does not move as far south, resulting in a weaker SASM. Persistent expressions of the positive or negative phase of the NAO have thus led to significant climatic anomalies in the past (Arnold et al., 2021). Studies have found correspondences between the periodicity of paleoclimatic conditions in the Peruvian Andes and the 65-year frequency of the AMOC (Apaéstegui et al., 2014).

So far, the large-scale climate oscillation signature of the LIA has remained relatively unclear outside the North Atlantic region (Mann et al., 2008). From our data, we suggest that the role of the Sun in modifying SH tropospheric circulation patterns needs to be reconsidered. Several studies attribute climate cooling during the LIA to solar forcing, particularly during the Wolf-, Spörer-, Maunder- and Dalton-Minima (Wanner et al., 2022; Brehm et al., 2021; Owens et al., 2017; Usoskin et al., 2015; Burn and Palmer, 2014). Volcanic forcing has also played an important role (Steinhilber et al., 2012) and features prominently in recent work (see Wanner et al., 2022). However, while volcanic eruptions have had a strong climatic impact, their influence on climate has been rather short-lived (Versteegh, 2005; Hegerl et al., 2003; Shindell et al., 2001). According to Helama et al. (2021), they can enhance cooling beyond a tipping point, leading to repeated Holocene cold climate events.

On a centennial scale, the evidence for solar-climate relationships in South America is clearly underrepresented. This is due to a lack of information and a lack of resolution in the archives, rather than a lack of response to solar forcing (Versteegh, 2005). Varma et al. (2011) showed that the XRF-measured iron contents of a marine core from the Chilean continental slope (41°S) are significantly correlated with reconstructed solar activity (Solanki et al., 2004) over the past 3000 years ($r = 0{,}45$ [0, 37; 0,53]). Our measured Ti/coh values show an even higher correlation ($r = -0{,}52$ [−0,38; −0,92]) compared to a new solar activity reconstruction (Steinhilber et al., 2009).

The correlation of the LC Ti/coh record with the solar activity minima and maxima is striking. Solar forcing appears to trigger the sedimentation characteristics of the chosen site, as changes in solar activity have a strong influence on regional precipitation rates via the modification of the SASM intensity. A stronger SASM provokes a stronger precipitation, which leads to a stronger erosion within the LC catchment and finally to a stronger lithic influx into the peat/organic sediment matrix. The size of the catchment that serves as the source area for the accumulated sediment at our study site, appears to be ideally suited to provide a very sensitive signal of precipitation-induced changes in the stratigraphic record. At too large a scale (e.g. large catchments of Andean lakes, glacial advance/retreat), more than one environmental parameter (such as grazing) may influence the proxy record, leading to underestimation or disappearance of the forcing (Versteegh, 2005).

Until now, the origin of the climate dynamics of the Central Andes during the last millennium has been speculative. On the basis of statistical evidence, we have identified solar variability as its origin. The interhemispheric climate link is based on the perturbation of the global heat balance. NH cooling due to solar forcing together with an increase in Arctic sea ice export weakens the AMOC, followed by an increase in southern tropical Atlantic sea surface temperatures, affecting the southward migration of the ITCZ (Schneider et al., 2014; Vuille et al., 2012). Proxy evidence documents such southward shifts of the ITCZ during cooling events in the NH, especially during pronounced events such as the LIA and the Younger Dryas (Bird et al., 2011; Haug et al., 2001). A more southerly position of the ITCZ triggers a moisture flux into the tropical lowlands, which enhances convective activity in the Amazon basin. As the main source of moisture in the tropical/subtropical Andes is the Amazon basin, it is suggested that the SASM intensity and central Andean precipitation are very sensitive to changes in NH temperatures (Vuille et al., 2012).

Moberg et al. (2005) reconstructed NH temperatures for the past 2000 years by combining low- and high resolution proxy data. They

suggested that much of the variability they detected could be due to a response to natural changes in radiative forcing. Indeed, the LC record shows a high correlation with the reconstructed NH temperatures of the last millennium (r = −0,66 [−0,32; −0,85]). Thus, the LC record clearly demonstrates the influence of NH temperature changes on the atmospheric circulation over tropical South America. The position of the ITCZ is robustly dependent on the interhemispheric temperature gradient (Schneider et al., 2014), triggered by solar forcing. The cooling of the LIA led systematically to a southward shift of the ITCZ and hence a strengthening of the SASM, resulting in an intensification of precipitation over the Peruvian Andes.

The dynamics of the SASM are additionally affected by the El Niño Southern Oscillation (ENSO). Strecker et al. (2007) summarize that stronger ENSO and/or regional ENSO influence may impact erosional processes in the central Andes. Enhanced oceanic sea surface temperature gradients during La Niña years lead to more frequent rainfall episodes through the strengthening and southward displacement of the BH and a subdued zonal upper level westerly circulation. Wet summers in the central Andes are associated with a La Niña-related cooling of the tropical Pacific, and thus, enhanced easterly flow (Vuille et al., 2000; Garreaud et al., 2003; Lücke et al., 2022). So far, comprehensive ENSO reconstructions yield conflicting results in the central Andes (Bustamante et al., 2016; Schneider et al., 2018; Kock et al., 2020). Discrepancies arise due to heterogenic interpretation of terrestrial and oceanic proxies as well as theoretical and physical models of predicted responses to global temperature changes (Barr et al., 2019). Multiple driving forces such as out-of-phase SASM modes (Vuille and Keimig, 2004), the ENSO, and the positioning of the ITCZ, contribute to a complex temporal modulation of the SASM response in the central Andes. This underscores the need for further research to fully understand the mechanisms at play and their implications for regional hydroclimate variability.

6. Conclusions

The high-resolution paleoclimate record from Laguna Comercocha (LC) has provided new data on climatic and environmental changes in the central Andes over the past millennium. Analysis of sediment cores revealed significant variability in climate on sub-centennial to interdecadal timescales, demonstrating that the region experienced substantial fluctuations in precipitation and geomorphodynamics. These results highlight the importance of understanding regional climate dynamics and their implications for Andean ecosystems, which are highly sensitive to climate variability.

Solar forcing emerged as an important driver of precipitation changes in the central Andes, particularly during the LIA. The study found that periods of increased lithogenic input during the LIA coincided with solar minima, suggesting a strong link between solar activity and regional precipitation patterns. The sediment core data also revealed important shifts in vegetation cover and geomorphodynamics, particularly after 1150 cal yr AD. This period marked the onset of increased precipitation, which had a significant impact on the local ecosystem. The MCA and the LIA were characterized by distinct climatic phases, with the MCA experiencing lower precipitation and the LIA showing increased variability and episodes of intense rainfall. These climatic changes were reflected in Ti/COH ratios and changes in pollen assemblages.

Overall, this study improves our understanding of paleoclimatic dynamics in the central Andes and provides a detailed perspective on last millennial climate variability. The results emphasize the need for continued research in this region, as they provide a crucial reference for future climate reconstructions and underline the complex interplay between solar activity, precipitation and environmental change in shaping the Andean landscape.

CRediT authorship contribution statement

Karsten Schittek: Writing – original draft, Visualization, Validation, Supervision, Project administration, Methodology, Investigation, Formal analysis, Data curation, Conceptualization. **Jan Wowrek:** Writing – review & editing, Visualization, Investigation, Funding acquisition, Formal analysis, Data curation. **Nicolas Käuffer:** Writing – review & editing, Investigation. **Markus Reindel:** Writing – review & editing, Project administration, Funding acquisition, Conceptualization. **Bertil Mächtle:** Writing – review & editing, Validation, Supervision, Project administration, Funding acquisition, Conceptualization.

Data availability

Raw data will be made available via PANGAEA – Data Publisher for Earth & Environmental Science.

Funding

This work was funded by the Innovation Fund Frontier (Heidelberg University) to BM, the Groundcheck Program of the German Archaeological Institute (DAI) to MR and the German Academic Exchange Service (DAAD) PROMOS scholarship to JW which is greatly appreciated.

Declaration of competing interest

The authors declare that they have no known competing financial interests or personal relationships that could have appeared to influence the work reported in this paper.

Acknowledgements

We thank Jonathan Hense, Alexander Reyes-Knoche and Fernando Leceta for great help during fieldwork. Special thanks belong to Liliana Lupo, Maria Eugenia de Porras and Antonio Maldonado for their help with the determination of pollen types. We also thank Sabine Stahl for support and help with the calibration of the XRF results and Susanne Lindauer for support and help with the radiocarbon ages.

References

Apaéstegui, J., Cruz, F.W., Sifeddine, A., Vuille, M., Espinoza, J.C., Guyot, J.L., Khodri, M., Strikis, N., Santos, R.V., Cheng, H., Edwards, L., Carvalho, E., Santini, W., 2014. Hydroclimate variability of the northwestern Amazon Basin near the Andean foothills of Peru related to the South American Monsoon System during the last 1600 years. Clim. Past 10 (6), 1967–1981. https://doi.org/10.5194/cp-10-1967-2014.

Arnold, T.E., Hillman, A.L., Abbott, M.B., Werne, J.P., McGrath, S.J., Arkush, E.N., 2021. Drought and the collapse of the tiwanaku civilization: new evidence from lake orurillo, Peru. Quat. Sci. Rev. 251, 106693. https://doi.org/10.1016/j.quascirev.2020.106693.

Autin, P., Sicart, J.E., Rabatel, A., Soruco, A., Hock, R., 2022. Climate controls on the interseasonal and interannual variability of the surface mass and energy balances of a tropical glacier (Zongo Glacier, Bolivia, 16° S): new insights from the multi-year application of a distributed energy balance. J. Geophys. Res. Atmos. 127 (7). https://doi.org/10.1029/2021JD035410 article no. e2021JD035410.

Balascio, N.L., Zhang, Z., Bradley, R.S., Perren, B., Dahl, S.O., Bakke, J., 2011. A multi-proxy approach to assessing isolation basin stratigraphy from the Lofoten Islands, Norway. Quat. Res. 75 (1), 288–300. https://doi.org/10.1016/j.yqres.2010.08.012.

Barr, C., Tibby, J., Leng, M.J., Tyler, J.J., Henderson, A.C.G., Overpeck, J.T., Simpson, J. L., Cole, J.E., Phipps, S.J., Marshall, J.C., McGregor, G.B., McRobie, F.H., 2019. Holocene El niño–southern oscillation variability reflected in subtropical Australian precipitation. Sci. Rep. 9, 1627. https://doi.org/10.1038/s41598-019-38626-3.

Blaauw, M., Christen, J.A., 2011. Flexible paleoclimate age-depth models using an autoregressive gamma process. Bayesian Analysis 6 (3). https://doi.org/10.1214/11-BA618.

Bird, B.W., Abbott, M.B., Vuille, M., Rodbell, D.T., Stansell, N.D., Rosenmeier, M.F., 2011. A 2,300-year-long annually resolved record of the South American summer monsoon from the Peruvian Andes. Proc. Natl. Acad. Sci. U.S.A. 108 (21), 8583–8588. https://doi.org/10.1073/pnas.1003719108.

Brehm, N., Bayliss, A., Christl, M., Synal, H.-A., Adolphi, F., Beer, J., Kromer, B., Muscheler, R., Solanki, S.K., Usoskin, I., Bleicher, N., Bollhalder, S., Tyers, C., Wacker, L., 2021. Eleven-year solar cycles over the last millennium revealed by

radiocarbon in tree rings. Nat. Geosci. 14 (1), 10–15. https://doi.org/10.1038/s41561-020-00674-0.ohlojl.
Burn, M.J., Palmer, S.E., 2014. Solar forcing of Caribbean drought events during the last millennium. J. Quat. Sci. 29 (8), 827–836. https://doi.org/10.1002/jqs.2660.
Bustamante, M.G., Cruz, F.W., Vuille, M., Apaéstegui, J., Strikis, N., Panizo, G., Novello, F.V., Deininger, M., Sifeddine, A., Cheng, H., Moquet, J.S., Guyot, J.L., Santos, R.V., Segura, H., Edwards, R.L., 2016. Holocene changes in monsoon precipitation in the Andes of NE Peru based on δ18O speleothem records. Quat. Sci. Rev. 146, 274–287. https://doi.org/10.1016/j.quascirev.2016.05.023.
Campos, M.C., Chiessi, C.M., Novello, V.F., Crivellari, S., Campos, J.L., Albuquerque, A.L. S., Venancio, I.M., Santos, T.P., Melo, D.B., Cruz, F.W., Sawakuchi, A.O., Mendes, V. R., 2022. South American precipitation dipole forced by interhemispheric temperature gradient. Sci. Rep. 12 (1), 10527. https://doi.org/10.1038/s41598-022-14495-1.
Carozza, J.M., Carozza, L., Valette, P., Llubes, M., Py, V., Galop, D., Danu, M., Ferdinand, L., David, M., Sévègnes, L., Bruxelles, L., Jarry, M., Duranthon, F., 2014. The subfossil tree deposits from the Garonne Valley and their implications on Holocene alluvial plain dynamics. Compt. Rendus Geosci. 346 (1–2), 20–27. https://doi.org/10.1016/j.crte.2014.01.001.
Croudace, I.W., Rindby, A., Rothwell, R.G., 2006. ITRAX: description and evaluation of a new multi-function X-ray core scanner. Geological Society, London, Special Publications 267 (1), 51–63. https://doi.org/10.1144/GSL.SP.2006.267.01.04.
Faegri, K., Iversen, J., 1989. Textbook of Pollen Analysis, fourth ed. The Blackburn Press, p. 340.
Flantua, S.G., Hooghiemstra, H., Vuille, M., Behling, H., Carson, J.F., Gosling, W.D., Hoyos, I., Ledru, M.P., Montoya, E., Mayle, F., Maldonado, A., Rull, V., Tonello, M.S., Whitney, B.S., González-Arango, C., 2016. Climate variability and human impact in South America during the last 2000 years: synthesis and perspectives from pollen records. Clim. Past 12 (2), 483–523. https://doi.org/10.5194/cp-12-483-2016.
Garreaud, R., Vuille, M., Clement, A.C., 2003. The climate of the Altiplano: observed current conditions and mechanisms of past changes. Palaeogeogr. Palaeoclimatol. Palaeoecol. 194 (1–3), 5–22. https://doi.org/10.1016/S0031-0182(03)00269-4.
Garreaud, R.D., Aceituno, P., 2001. Interannual rainfall variability over the South american Altiplano. J. Clim. 14 (12), 2779–2789. https://doi.org/10.1175/1520-0442(2001)014<2779:IRVOTS>2.0.CO, 2.
Garreaud, R.D., Aceituno, P., 2007. Atmospheric circulation and climatic variability. The physical geography of South America 45, 59.
Graf, K., 1979. Untersuchungen zur rezenten Pollen- und Sporenflora in der nördlichen Zentralkordillere Boliviens und Versuch einer Auswertung von Profilen aus postglazialen Torfmooren. Zürich.
Graf, K., 1981. Palynological investigations of two post-glacial peat bogs near the boundary of Boliva and Peru. J. Biogeogr. 8, 353–368.
Graf, K., 1986. Klima und Vegetationsgeschichte der Anden, 19. Physische Geographie, Zürich.
Grimm, E.C., 1987. CONISS: a FORTRAN 77 program for stratigraphically constrained cluster analysis by the method of incremental sum of squares. Comput. Geosci. 13 (1), 13–35.
Haug, G.H., Hughen, K.A., Sigman, D.M., Peterson, L.C., Röhl, U., 2001. Southward migration of the intertropical convergence zone through the Holocene. Science (New York, N.Y.) 293 (5533), 1304–1308. https://doi.org/10.1126/science.1059725.
Hegerl, G.C., Crowley, T.J., Baum, S.K., Kim, K.-Y., Hyde, W.T., 2003. Detection of volcanic, solar and greenhouse gas signals in paleo-reconstructions of Northern Hemispheric temperature. Geophys. Res. Lett. 30 (5), 2002GL016635. https://doi.org/10.1029/2002GL016635.
Helama, S., Stoffel, M., Hall, R.J., Jones, P.D., Arppe, L., Matskovsky, V.V., Timonen, M., Nöjd, P., Mielikäinen, K., Oinonen, M., 2021. Recurrent transitions to little ice age-like climatic regimes over the Holocene. Clim. Dynam. 56 (11–12), 3817–3833. https://doi.org/10.1007/s00382-021-05669-0.
Heusser, C.J., 1971. Pollen and Spores of Chile. Modern Types of the Pteridophyta, Gymnospermae and Angospermae. Arizona.
Hurrell, J.W., Kushnir, Y., Visbeck, M., 2001. The North atlantic oscillation. Science 603–605. https://doi.org/10.1126/science.1058761, 2001.
Jara, I.A., Maldonado, A., Eugenia de Porras, M., 2020. Late Holocene dynamics of the South American summer monsoon: new insights from the Andes of northern Chile (21°S). Quat. Sci. Rev. 246, 106533. https://doi.org/10.1016/j.quascirev.2020.106533.
Jomelli, V., Swingedouw, D., Vuille, M., Favier, V., Goehring, B., Shakun, J., Braucher, R., Schimmelpfennig, I., Menviel, L., Rabatel, A., Martin, L.C.P., Blard, P. H., Condom, T., Lupker, M., Christl, M., He, Z., Verfaillie, D., Gorin, A., Aumaître, G., Bourlès, D.L., Keddadouche, K., 2022. In-phase millennial-scale glacier changes in the tropics and North Atlantic regions during the Holocene. Nat. Commun. 13 (1), 1419. https://doi.org/10.1038/s41467-022-28939-9.
Jones, P.D., Mann, M.E., 2004. Climate over past millennia. Rev. Geophys. 42 (2). https://doi.org/10.1029/2003RG000143.
Kock, S.T., Schittek, K., Wissel, H., Vos, H., Ohlendorf, C., Schäbitz, F., Lupo, L.C., Kulemeyer, J.J., Lücke, A., 2019. Stable oxygen isotope records (δ18O) of a high-andean cushion peatland in NW Argentina (24° S) imply South American summer monsoon related moisture changes during the late Holocene. Front. Earth Sci. 7, 45. https://doi.org/10.3389/feart.2019.00045.
Kock, S.T., Schittek, K., Mächtle, B., Maldonado, A., Vos, H., Lupo, L.C., Kulemeyer, J.J., Wissel, H., Schäbitz, F., Lücke, A., 2020. Multi-centennial-scale variations of South American summer monsoon intensity in the southern central Andes (24–27°S) during the late Holocene. Geophys. Res. Lett. 47, e2019GL084157. https://doi.org/10.1029/2019GL084157.
Körner, C., 2012. High elevation treelines. Alpine Treelines: Functional Ecology of the Global High Elevation Tree Limits, pp. 1–10.
Kuentz, A., Ledru, M.P., Thouret, J.C., 2012. Environmental changes in the highlands of the western Andean Cordillera, southern Peru, during the Holocene. Holocene 22 (11), 1215–1226. https://doi.org/10.1177/0959683611409772.
Kuhlbrodt, T., Griesel, A., Montoya, M., Levermann, A., Hofmann, M., Rahmstorf, S., 2007. On the driving processes of the Atlantic meridional overturning circulation. Rev. Geophys. 45 (2). https://doi.org/10.1029/2004RG000166.
Ledru, M.-P., Jomelli, V., Samaniego, P., Vuille, M., Hidalgo, S., Herrera, M., Ceron, C., 2013. The medieval climate anomaly and the little ice age in the eastern Ecuadorian Andes. Clim. Past 9 (1), 307–321. https://doi.org/10.5194/cp-9-307-2013.
Licciardi, J.M., Schaefer, J.M., Taggart, J.R., Lund, D.C., 2009. Holocene glacier fluctuations in the Peruvian Andes indicate northern climate linkages. Science (New York, N.Y.) 325 (5948), 1677–1679. https://doi.org/10.1126/science.1175010.
Liu, K., Reese, C.A., Thompson, L.G., 2005. Ice-core pollen record of climatic changes in the central Andes during the last 400 yr. Quat. Res. 64 (2), 272–278. https://doi.org/10.1016/j.yqres.2005.06.001.
Lücke, A., Kock, S., Wissel, H., Kulemeyer, J.J., Lupo, L.C., Schäbitz, F., Schittek, K., 2022. Hydroclimatic record from an Altiplano cushion peatland (24° S) indicates large-scale reorganization of atmospheric circulation for the late Holocene. PLoS One 17 (11), e0277027. https://doi.org/10.1371/journal.pone.0277027.
Markgraf, V., D'Antoni, H.L., 1978. Pollen Flora of Argentina. Modern Spore and Pollen Types of Pteridophyta, Gymnospermae, and Angiospermae.
Mann, M.E., Bradley, R.S., Crespin, E., Goosse, H., Hughes, M.K., Rutherford, S., Shindell, D., Zhang, Z., 2008. Towards understanding patterns of climate change in past centuries. Eos, Transactions American Geophysical Union 89 (53).
Mann, M.E., Zhang, Z., Rutherford, S., Bradley, R.S., Hughes, M.K., Shindell, D., Ammann, C., Faluvegi, G., Ni, F., 2009. Global signatures and dynamical origins of the little ice age and medieval climate anomaly. Sci. Technol. Humanit. 326 (5957), 1256–1260. https://doi.org/10.1126/science.1177303.
Martel-Cea, A., Maldonado, A., de Porras, M.E., Muñoz, P., Maidana, N.I., Massaferro, J., Schittek, K., 2023. A multiproxy approach to reconstruct the Late Holocene environmental dynamics of the semiarid Andes of central Chile (29° S). Frontiers in Ecology and Evolution 11, 1227020. https://doi.org/10.3389/fevo.2023.1227020.
Metcalfe, S.E., Jones, M.D., Davies, S.J., Noren, A., Mackenzie, A., 2010. Climate variability over the last two millennia in the North American Monsoon region, recorded in laminated lake sediments from Laguna de Juanacatlan, Mexico. Holocene 20, 1195–1206. https://doi.org/10.1177/0959683610371994.
Moberg, A., Sonechkin, D.M., Holmgren, K., Datsenko, N.M., Karlén, W., Lauritzen, S.-E., 2005. Highly variable Northern Hemisphere temperatures reconstructed from low- and high-resolution proxy data. Nature 433 (7026), 613–617. https://doi.org/10.1038/nature03265.
Moffa-Sánchez, P., Born, A., Hall, I.R., Thornalley, D.J., Barker, S., 2014. Solar forcing of North Atlantic surface temperature and salinity over the past millennium. Nat. Geosci. 7 (4), 275–278. https://doi.org/10.1038/ngeo2094.
Morales, M.S., Christie, D.A., Villalba, R., Argollo, J., Pacajes, J., Silva, J.S., Alvarez, C. A., Llancabure, J.C., Soliz Gamboa, C.C., 2012. Precipitation changes in the South American Altiplano since 1300 AD reconstructed by tree-rings. Clim. Past 8 (2), 653–666. https://doi.org/10.5194/cp-8-653-2012.
Muller, J., Kylander, M., Wüst, R.A.J., Weiss, D., Martinez Cortizas, A., LeGrande, A.N., Jennerjahn, T., Behling, H., Anderson, W.T., Jacobson, G., 2008. Possible evidence for wet Heinrich phases in tropical NE Australia: the Lynch's Crater deposit. Quat. Sci. Rev. 27, 468–475. https://doi.org/10.1016/j.quascirev.2007.11.006.
Novello, V.F., Cruz, F.W., Moquet, J.S., Vuille, M., Paula, M. S. de, Nunes, D., Edwards, R. L., Cheng, H., Karmann, I., Utida, G., Stríkis, N.M., Campos, J.L.P.S., 2018. Two millennia of South Atlantic convergence zone variability reconstructed from isotopic proxies. Geophys. Res. Lett. 45 (10), 5045–5051. https://doi.org/10.1029/2017GL076838.
Novoselov, A.A., Silva, D., de Souza Filho, C.R., 2020. Authigenic titanite in weathered basalts: implications for paleoatmospheric reconstructions. Geosci. Front. 11 (6), 2183–2196. https://doi.org/10.1016/j.gsf.2020.03.012.
Ohlendorf, C., Fey, M., Gebhardt, C., Haberzettl, T., Lücke, A., Mayr, C., Schäbitz, F., Wille, M., Zolitschka, B., 2013. Mechanisms of lake-level change at Laguna Potrok Aike (Argentina) – insights from hydrological balance calculations. Quat. Sci. Rev. 71, 27–45. https://doi.org/10.1016/j.quascirev.2012.10.040.
Owens, M.J., Lockwood, M., Hawkins, E., Usoskin, I., Jones, G.S., Barnard, L., et al., 2017. The Maunder minimum and the Little Ice Age: an update from recent reconstructions and climate simulations. Journal of Space Weather and Space Climate 7, A33. https://doi.org/10.1051/swsc/2017034.
Polanco-Martínez, J.M., Medina-Elizalde, M.A., Sánchez Goñi, M.F., Mudelsee, M., 2019. BINCOR: an R package for estimating the correlation between two unevenly spaced time series. RELC J. 11, 170–184. https://doi.org/10.32614/RJ-2019-035.
Polissar, P.J., Abbott, M.B., Wolfe, A.P., Bezada, M., Rull, V., Bradley, R.S., 2006. Solar modulation of little ice age climate in the tropical Andes. Proc. Natl. Acad. Sci. USA 103 (24), 8937–8942. https://doi.org/10.1073/pnas.0603118103.
R Core Team, R, 2013. R: A Language and Environment for Statistical Computing.
Reimer, P.J., Austin, W.E., Bard, E., Bayliss, A., Blackwell, P.G., Ramsey, C.B., Butzin, M., Cheng, H., Lawrence Edwards, R., Talamo, S., 2020. The IntCal20 Northern Hemisphere radiocarbon age calibration curve (0–55 cal kBP). Radiocarbon 62 (4), 725–757. https://doi.org/10.1017/RDC.2020.41.
Reutter, J., Stott, L., Khider, D., Sinha, A., Cheng, H., Edwards, R.L., 2009. A new perspective on the hydroclimate variability in northern South America during the Little Ice Age. Geophys. Res. Lett. 36 (21). https://doi.org/10.1029/2009GL041051. Art. 2009GL041051.
Rodbell, D.T., Seltzer, G.O., Mark, B.G., Smith, J.A., Abbott, M.B., 2008. Clastic sediment flux to tropical Andean lakes: records of glaciation and soil erosion. Quat. Sci. Rev. 27 (15–16), 1612–1626. https://doi.org/10.1016/j.quascirev.2008.06.004.

Rothwell, R.G., Croudace, I.W., 2015. Micro-XRF studies of sediment cores: a perspectiveon capability and application in the environmental sciences. In: Croudace, I.W., Rothwell, R.G. (Eds.), Micro-XRF Studies of Sediment Cores. Springer, Dordrecht, pp. 1–21.

Ruthsatz, B., 2012. Vegetación y ecología de los bofedales altoandinos de Bolivia (Vegetation and ecology of the high Andean peatlands of Bolivia). Phytocoenologia 42 (3–4), 133–179. https://doi.org/10.1127/0340-269X/2012/0042-0535.

Sanchez, F.A., Zapata, M.A., 2003. Memoria descriptive de la revision y actualización de los quadrángulos de Sicuani (29-t), NuNNoa (29-u), Macusani (29-v), Limbani (29-x), Sandia (29-y), San Ignacio (29-z), Yauri (30-t), Azángaro (30-v), Putina (30-x), La Riconada (30-y), Condoroma (31-t), Ocuviri (31-u), Juliaca (31-v) Callalli (32-t), Ácora (32-x). INEMMET, Lima. 55p.

Sandoval, A.P., Marconi, L., Ortuño, 2010. Flora Polínica de Bofedales y áreas aledañas del Tuni Condoriri. La Paz-Bolivia.

Schittek, K., 2014. Cushion peatlands in the high Andes of northwestern Argentina as archives for palaeoenvironmental research. In: Dissertationes Botanicae, 412. Schweizerbart Science Publishers, Stuttgart.

Schittek, K., Forbriger, M., Mächtle, B., Schäbitz, F., Wennrich, V., Reindel, M., Eitel, B., 2015. Holocene environmental changes in the highlands of the southern Peruvian Andes (14° S) and their impact on pre-Columbian cultures. Clim. Past 11 (1), 27–44. https://doi.org/10.5194/cp-11-27-2015.

Schittek, K., Kock, S.T., Lücke, A., Hense, J., Ohlendorf, C., Kulemeyer, J.J., Lupo, L.C., Schäbitz, F., 2016. A high-altitude peatland record of environmental changes in the NW Argentine Andes (24 ° S) over the last 2100 years. Clim. Past 12 (5), 1165–1180. https://doi.org/10.5194/cp-12-1165-2016.

Schittek, K., Forbriger, M., Berg, D., Hense, J., Schäbitz, F., Eitel, B., 2018. Last millennial environmental dynamics in the western Peruvian Andes inferred from the development of a cushion-plant peat hillock. Perspect. Plant Ecol. Evol. Systemat. 30, 115–124. https://doi.org/10.1016/j.ppees.2017.09.002.

Schittek, K., Teichert, L., Geiger, K., Knorr, K.H., Schneider, S., 2021. A 14,000 year peatland record of environmental change in the southern Gutland region, Luxembourg. Holocene 31 (6), 1005–1018. https://doi.org/10.1177/0959683621994645.

Schneider, T., Bischoff, T., Haug, G.H., 2014. Migrations and dynamics of the intertropical convergence zone. Nature 513 (7516), 45–53. https://doi.org/10.1038/nature13636.

Schneider, T., Hampel, H., Mosquera, P.V., Tylmann, W., Grosjean, M., 2018. Paleo-ENSO revisited: Ecuadorian Lake Pallcacocha does not reveal a conclusive El Niño signal. Global Planet. Change 168, 54–66. https://doi.org/10.1016/j.gloplacha.2018.06.004.

Segura, H., Espinoza, J.C., Junquas, C., Lebel, T., Vuille, M., Garreaud, R., 2020. Recent changes in the precipitation-driving processes over the southern tropical Andes/western Amazon. Clim. Dynam. 54 (5), 2613–2631. https://doi.org/10.1007/s00382-020-05132-6.

Shindell, D.T., Schmidt, G.A., Mann, M.E., Rind, D., Waple, A., 2001. Solar forcing of regional climate change during the Maunder Minimum. Science 294 (5549), 2149–2152. https://doi.org/10.1126/science.1064363. New York, N.Y.

Solanki, S.K., Usoskin, I.G., Kromer, B., Schüssler, M., Beer, J., 2004. Unusual activity of the Sun during recent decades compared to the previous 11,000 years. Nature 431 (7012), 1084–1087. https://doi.org/10.1038/nature02995.

Solomina, O.N., Bradley, R.S., Hodgson, D.A., Ivy-Ochs, S., Jomelli, V., Mackintosh, A.N., Atle, Nesje, Lewis, A. Owen, Heinz, Wanner, Wiles, Gregory C., Young, N.E., 2015. Holocene glacier fluctuations. Quat. Sci. Rev. 111, 9–34. https://doi.org/10.1016/j.quascirev.2014.11.018.

Stansell, N.D., Rodbell, D.T., Abbott, M.B., Mark, B.G., 2013. Proglacial lake sediment records of Holocene climate change in the western Cordillera of Peru. Quat. Sci. Rev. 70, 1–14. https://doi.org/10.1016/j.quascirev.2013.03.003.

Steinhilber, F., Beer, J., Fröhlich, C., 2009. Total solar irradiance during the Holocene. Geophys. Res. Lett. 36 (19), GL040142. https://doi.org/10.1029/2009GL040142.

Steinhilber, F., Abreu, J.A., Beer, J., Brunner, I., Christl, M., Fischer, H., Heikkilä, U., Kubik, P.W., Mann, M., McCracken, K.G., Miller, H., Miyahara, H., Oerter, H., Wilhelms, F., 2012. 9,400 years of cosmic radiation and solar activity from ice cores and tree rings. Proc. Natl. Acad. Sci. U.S.A. 109 (16), 5967–5971. https://doi.org/10.1073/pnas.1118965109.

Strecker, M.R., Alonso, R.N., Bookhagen, B., Carrapa, B., Hilley, G.E., Sobel, E.R., Trauth, M.H., 2007. Tectonics and climate of the southern central Andes. Annu. Rev. Earth Planet Sci. 35, 747–787. https://doi.org/10.1146/annurev.earth.35.031306.140158.

Stroup, J.S., Kelly, M.A., Lowell, T.V., Applegate, P.J., Howley, J.A., 2014. Late Holocene fluctuations of qori kalis outlet glacier, Quelccaya ice cap, Peruvian Andes. Geology 42 (4), 347–350. https://doi.org/10.1130/G35245.1.

Taugourdeau, O., 2006. Atlas de quelques grains de pollen du Pérou, En particulier de la region du Nevado Coropuna. Montpellier.

Thompson, L.G., Mosley-Thompson, E., Dansgaard, W., Grootes, P.M., 1986. The Little Ice Age as recorded in the stratigraphy of the tropical Quelccaya ice cap. Science 234 (4774), 361–364. https://doi.org/10.1126/science.234.4774.361.

Thompson, L.G., Mosley-Thompson, E., Brecher, H., Davis, M., Leon, B., Les, D., Lin, P.N., Mashiotta, T., Mountain, K., 2006. Abrupt tropical climate change: past and present. Proc. Natl. Acad. Sci. USA 103 (28), 10536–10543. https://doi.org/10.1073/pnas.0603900103.

Thompson, L.G., Mosley-Thompson, E., Davis, M.E., Zagorodnov, V.S., Howat, I.M., Mikhalenko, V.N., Lin, P.-N., 2013. Annually resolved ice core records of tropical climate variability over the past ~1800 years. Science (New York, N.Y.) 340 (6135), 945–950. https://doi.org/10.1126/science.1234210.

Thomson, J., Croudace, I.W., Rothwell, R.G., 2006. A geochemical application of the ITRAX scanner to a sediment core containing eastern Mediterranean sapropel units. Geological Society, London, Special Publications 267 (1), 65–77. https://doi.org/10.1144/GSL.SP.2006.267.01.05.

Torres, G.R., Lupo, L.L., Sánchez, A.C., Schittek, K., 2012. Contributions to the pollen flora of high-Andean cushion peatlands, Jujuy Province, Northwestern Argentina. Gayanna Botanica 69, 30–36. https://doi.org/10.4067/S0717-66432012000100004.

Usoskin, I.G., Arlt, R., Asvestari, E., Hawkins, E., Käpylä, M., Kovaltsov, G.A., Krivova, N., Lockwood, M., Mursula, K., O'Reilly, J., Owens, M., Scott, C.J., Sokoloff, D.D., Solanki, S.K., Soon, W., Vaquero, J.M., 2015. The Maunder minimum (1645–1715) was indeed a grand minimum: a reassessment of multiple datasets. Astron. Astrophys. 581, A95. https://doi.org/10.1051/0004-6361/201526652.

van der Bilt, W.G., Bakke, J., Vasskog, K., D'Andrea, W.J., Bradley, R.S., Ólafsdóttir, S., 2015. Reconstruction of glacier variability from lake sediments reveals dynamic Holocene climate in Svalbard. Quat. Sci. Rev. 126, 201–218. https://doi.org/10.1016/j.quascirev.2015.09.003.

van der Bilt, W.G.M., Bakke, J., Werner, J.P., Paasche, Ø., Rosqvist, G., Vatle, S.S., 2017. Late Holocene glacier reconstruction reveals retreat behind present limits and two-stage Little Ice Age on subantarctic South Georgia. J. Quat. Sci. 32 (6), 888–901. https://doi.org/10.1002/jqs.2937.

Varma, V., Prange, M., Lamy, F., Merkel, U., Schulz, M., 2011. Solar-forced shifts of the southern Hemisphere westerlies during the Holocene. Clim. Past 7 (2), 339–347. https://doi.org/10.5194/cp-7-339-2011.

Vera, C., Higgins, W., Amador, J., Ambrizzi, T., Garreaud, R., Gochis, D., Gutzler, D., Lettenmaier, D., Marengo, J., Mechoso, C.R., Nogues-Paegle, J., Silva Dias, P.L., Zhang, C., 2006. Toward a unified view of the American monsoon systems. J. Clim. 19 (20), 4977–5000. https://doi.org/10.1175/JCLI3896.1.

Versteegh, G.J.M., 2005. Solar forcing of climate. 2: evidence from the past. Space Sci. Rev. 120 (3–4), 243–286. https://doi.org/10.1007/s11214-005-7047-4.

Vuille, M., Keimig, F., 2004. Interannual variability of summertime convective cloudiness and precipitation in the central Andes derived from ISCCP-B3 data. J. Clim. 17 (17), 3334–3348. https://doi.org/10.1175/1520-0442(2004)017<3334:IVOSCC>2.0.CO, 2.

Vuille, M., Bradley, R.S., Keimig, F., 2000. Climate variability in the Andes of Ecuador and its relation to tropical Pacific and Atlantic sea surface temperature anomalies. J. Clim. 13 (14), 2520–2535. https://doi.org/10.1175/1520-0442(2000)013<2520:CVITAO>2.0.CO, 2.

Vuille, M., Burns, S.J., Taylor, B.L., Cruz, F.W., Bird, B.W., Abbott, M.B., Kanner, L.C., Cheng, H., Novello, V.F., 2012. A review of the South American monsoon history as recorded in stable isotopic proxies over the past two millennia. Clim. Past 8 (4), 1309–1321. https://doi.org/10.5194/cp-8-1309-2012.

Wanner, H., Solomina, O., Grosjean, M., Ritz, S.P., Jetel, M., 2011. Structure and origin of Holocene cold events. Quat. Sci. Rev. 30 (21–22), 3109–3123. https://doi.org/10.1016/j.quascirev.2011.07.010.

Wanner, H., Pfister, C., Neukom, R., 2022. The variable European little ice age. Quat. Sci. Rev. 287, 107531. https://doi.org/10.1016/j.quascirev.2022.107531.

White, A.F., Peterson, M.L., Hochella, M.F., 1994. Electrochemistry and dissolution kinetics of magnetite and ilmenite. Geochem. Cosmochim. Acta 58 (8), 1859–1875.

Wingenroth, M., Heusser, C.J., 1985. Pollen of the High Andean Flora: Quebrada Benjamin Matienzo, Province of Mendoza, Argentina. Instituto Argentino de Nivología y Glaciología.